Chemical Engineering Journal 308 (2017) 1225–1232

Contents lists available at ScienceDirect

Chemical Engineering Journal

journal homepage: www.elsevier.com/locate/cej

First principles study of adsorption and oxidation mechanism of elemental mercury by HCl over MoS_2 (1 0 0) surface

Zhenming Xu [a], Xiaojun Lv [a,*], Jiangan Chen [b], Liangxing Jiang [a], Yanqing Lai [a], Jie Li [a]

[a] School of Metallurgy and Environment, Central South University, Changsha 410083, China
[b] Faculty of Resource and Environmental Engineering, Jiangxi University of Science and Technology, Ganzhou 341000, China

HIGHLIGHTS

- HCl adsorption on MoS_2 (1 0 0) is a chemical dissociated process.
- HgCl and $HgCl_2$ are dissociatively adsorbed, while non-dissociatively adsorbed.
- Hg oxidation on the MoS_2 (1 0 0) obeys the Langmuir–Hinshelwood mechanism.
- The formation of HgCl and dissociation of $HgCl_2$ are the rate-determining steps.
- MoS_2 is an attractive alternative catalyst for Hg oxidation.

ARTICLE INFO

Article history:
Received 5 July 2016
Received in revised form 7 September 2016
Accepted 14 October 2016
Available online 24 October 2016

Keywords:
Density functional theory
Mercury
Molybdenum disulfide
Adsorption
Oxidation mechanism

ABSTRACT

The Hg oxidation mechanism by HCl over MoS_2 (1 0 0) surface was firstly investigated by the density functional theory and the periodic slab model. Hg^0 is strongly adsorbed on the Mo top site of MoS_2 (1 0 0) surface due to the overlaps between the *s*, *p* state of Hg atom and the *s*, *p* state of Mo atom. The H–Cl bond of the isolated HCl molecule is destroyed after adsorption on the MoS_2 (1 0 0) surface, revealing a chemical dissociated adsorption process. HgCl and $HgCl_2$ is dissociatively adsorbed on the Mo top site, while non-dissociatively adsorbed on the S edge site of MoS_2 (1 0 0) surface. Energy pathway analysis indicates that Hg^0 oxidation on the MoS_2 (1 0 0) surface obeys the Langmuir–Hinshelwood mechanism via the pathway of Hg → HgCl → $HgCl_2$. In the whole Hg oxidation reaction, the formation of HgCl and the dissociation of $HgCl_2$ are the rate-determining steps due to their high energy barriers. The lower energy barrier of the mercury oxidation reaction on MoS_2 surface makes it an attractive alternative catalyst for Hg catalytic oxidation.

1. Introduction

Mercury pollution is of great concern for public due to its high toxicity, volatility and bioaccumulation [1–3]. One of the main sources of mercury emission is coal combustion in the thermal power plants [4]. In 2011, the Ministry of Environmental Protection of China executed the effluent standard of hazardous air pollutants from the coal-fired power plants, in which the upper limit of mercury effluent is set to 0.03 mg/m^3. Moreover, in 2013, the Environmental Protection Agency of the United States reinforced the effluent restrictions of mercury and other poisonous gas pollutants for the new power plants, which is not exceeding 0.003 lb/MW h (pounds pollutant per megawatt-hour electric output) [5]. In the flue gas, according to the combustion conditions and the coals chlorine content, the existence form of mercury are mainly divided into three cases of elemental mercury (Hg^0), oxidized mercury (Hg^{2+}), and particulate mercury (Hg_p) [6]. Oxidized mercury (Hg^{2+}) can dissolve in water by the wet flue gas desulfurization system. In addition, particulate mercury is also easy to be trapped with the dust collection equipment. However, for case of Hg^0, low solubility in water and high volatility make it is neither water-soluble nor easily adsorbed on the solid surface to form particulate mercury [7]. More seriously, the closed electron structure of $5d^{10}6s^2$ makes elemental mercury (Hg^0) chemical inert for oxidation even in the gas phase full of oxygen [8]. Therefore, developing relevant technologies to reduce the mercury effluent from coal-fired power plants is an impending concern.

To date, the main methods for elemental mercury removal are divided into two types: one is adsorption on the solid surface to form particulate mercury, and the other is catalytic oxidation of

* Corresponding author at: School of Metallurgy and Environment, Central South University, No. 932, South Road Lushan, Changsha, Hunan 410083, China.
E-mail address: lvxiaojun@csu.edu.cn (X. Lv).

http://dx.doi.org/10.1016/j.cej.2016.10.059
1385-8947/

Hg^0 to Hg^{2+} subsequently dissolved in water by a wet flue gas desulfurization system [7]. Correspondingly, fly ash [9,10], lime [11], activated carbon [12–17], metallic oxide [18], even precious metals [5,19–22] were widely investigated as the promising adsorbents for the removal of elemental mercury. In addition, many kinds of catalysts have been developed for mercury oxidation, such as carbon-based catalysts [6,23], metal and metal oxide catalysts-based [24–30], selective catalytic reduction (SCR) catalysts [31,32]. Among these developed catalysts, Pd-based materials attracted the attention of many researchers, which shows good performances of high efficiency of mercury removal, regeneration and high activity after long time service. Researchers around the world are constantly searching for highly efficient adsorbents and catalysts for elemental mercury removal.

Recently, the large-area graphene-like molybdenum disulfide (MoS_2) has been synthesized experimentally [33–35]. A novel quasi-two-dimensional layered material, is a promising candidate as an adsorbent and catalyst for mercury removal at room temperature due to its special layered structure, large surface areas and strong covalent forces with van der Waals interactions [34–36]. Recently, the research studies of MoS_2 in the fields of hydrogen evolution [37], lithium and sodium battery performance [38–40], K promoted on MoS_2 catalysts [41,42], etc. are also gaining increasing scientific interest. Some published researches also reveal that outstanding adsorption performance of MoS_2 is exhibited in the removal of aromatic sulfur compounds from fuel [43] and doxycycline antibiotic from aqueous solution [44]. Moreover, water-gas-shift reaction over sulfur covered MoS_2 (1 0 0) surfaces was investigated by Shi et al. with the density functional theory (DFT) [45]. Zhao et al. [46] have investigated the mercury capture over $CoMoS/\gamma\text{-}Al_2O_3$ with MoS_2 nanosheets at low temperatures, which achieved almost 100% mercury removal efficiency at 50 °C. Raybaud et al. have studied the MoS_2-based hydrodesulfurization catalysts by DFT calculations [47–50], and pointed out that the S-terminated ($\bar{1}$ 0 1 0) edge sites own the highest catalytic activity. Inspired by the excellent catalytic performances of MoS_2, a question hanging on our head that whether it is likely to apply MoS_2 for the mercury adsorption and catalytic oxidation? However, its adsorption and catalytic oxidation mechanism of mercury pollutants removal has not been reported till now.

In this study, to explore the mechanism of adsorption and catalytic oxidation of mercury on MoS_2 surface from flue gas at low temperatures. To figure out the mercury oxidation mechanism on MoS_2 (1 0 0) surfaces, the first-principles calculations based on the density functional theory (DFT) were carried out. The possible reaction pathways were investigated in detail, including the adsorptions of reactants (Hg^0 and HCl), the dissociation of HCl, and the formation and desorption of HgCl and $HgCl_2$. Additionally, the transition states and intermediates during these reaction pathways were also located, and the corresponding energy barriers of the elementary mercury oxidation reactions were examined.

2. Computational methodology and models

In this work, all calculations were performed using the density functional theory (DFT) with exchange-correlation functional GGA-PBE [51] as implemented in the CASTEP package [52]. Ultrasoft pseudo potentials (USPP) introduced by Vanderbilt [53] have been employed for all ion-electron interactions. The Mo $4p^6 4d^5 5s^1$, S $3s^2 3p^4$, Hg $5d^{10} 6s^2$, H $1s^1$ and Cl $3s^2 3p^5$ electrons were explicitly treated as valence electrons. Convergence with respect to both energy cutoff and *k*-point mesh have been tested. As a result of convergence (Table S1 in Supporting Information), an energy cutoff of 500 eV and $6 \times 6 \times 2$ *k*-points mesh using the method of Monkhorst–Pack [54] was chosen to ensure that total energy of molybdenum disulfide crystal was converged within 1×10^{-4} eV/atom. For all following supercell calculations, *k*-point meshes with the same density as the unit cell were used. Moreover, the energy convergence criterion for self-consistent field (SCF) calculation was set to 1×10^{-6} eV/atom.

In order to locate the most-stable configuration of clean MoS_2 and adsorbate covered MoS_2 surface, atoms and cell optimization were performed using total energy minimization methods. The total-energy difference was within 10^{-6} eV/atom, the maximum force was within 10^{-4} eV/Å, the maximum stress was within 0.01 GPa and the maximum atom displacement was within 10^{-4} Å. Two-dimensional periodic boundary conditions were still introduced to these surface calculations for adsorbed MoS_2. Moreover, a vacuum region of 20 Å was also applied in the direction perpendicular to the adsorbed MoS_2 plane to eliminate the interactions between adjacent conformations. The stability of the adsorbed MoS_2 system can be estimated by its average adsorption energy (ΔE). For example, in the Hg adsorbed MoS_2 system, the average adsorption energy was calculated according to the following equation [55]:

$$\Delta E = [E(MoS_2 \text{adsorbed Hg}) - (E(MoS_2) + E\ (Hg))] \quad (1)$$

where E (MoS_2 adsorbed Hg), E (MoS_2) and E (Hg) is total energies of the Hg adsorbed MoS_2 system, the MoS_2 (1 0 0) surface and a single Hg atom, respectively.

The linear synchronous transit/quadratic synchronous transit (LST/QST) combined with conjugate gradient (CG) method refinements method was employed for the calculation of energy barriers of transition states (TS) and intermediates (IM) during the elementary mercury oxidation reactions [56]. In addition, TS confirmations were conducted by the nudged elastic band (NEB) method [57].

3. Results and discussion

3.1. Hg^0 adsorption on MoS_2 (1 0 0) surface

To simulate the mercury adsorption at low concentration on the MoS_2 (1 0 0) surface, on which the Hg–Hg interactions can weaken with the lower surface coverage, the periodic model of $p(4 \times 1)$ MoS_2 (1 0 0) surface slab adsorbed with a single Hg atom was used. We have tested the size of period adsorption slab by calculating the convergence adsorption energy of a single Hg atom on the Mo top adsorption site of MoS_2 (1 0 0) surface. Convergence with the size of period adsorption slab has been provided in Table S2 in Supporting Information. It is found that the single Hg adsorption energy indeed converges to a size of $p(4 \times 1)$ unit cell with a largest adsorption energy of −1.66 eV/Hg atom. The bulk structure of MoS_2 was then cleaved along the (1 0 0) plane, generating a Mo-terminated (1 0 $\bar{1}$ 0) edge and an S-terminated ($\bar{1}$ 0 1 0) edge. A single Hg adatom was initially placed on the top site of Mo and S atom on the Mo and S edge of the MoS_2 (1 0 0) surface, respectively, and then full optimizations of the fractional coordinates for these periodic absorption slabs were carried out. The optimized configurations of mercury adsorption are depicted in Fig. 1a and b. The calculated results of adsorption energy, bond length, Mulliken charge, and bond population of the MoS_2 (1 0 0) surface system absorbed with Hg are listed in Table 1.

The calculated result of adsorption energy shows that the strength of Hg adsorption follows this order: Mo top site >S top site. The Mo top site of MoS_2 (1 0 0) surface is more energetically preferred for Hg adsorption with a larger adsorption energy of −1.66 eV/atom(Hg) on the periodic $p(4 \times 1)$ slab, and the corresponding adsorption bond length of Hg–Mo is 2.76 Å. All the Mulliken charges of Hg atoms are positive, indicating more or less

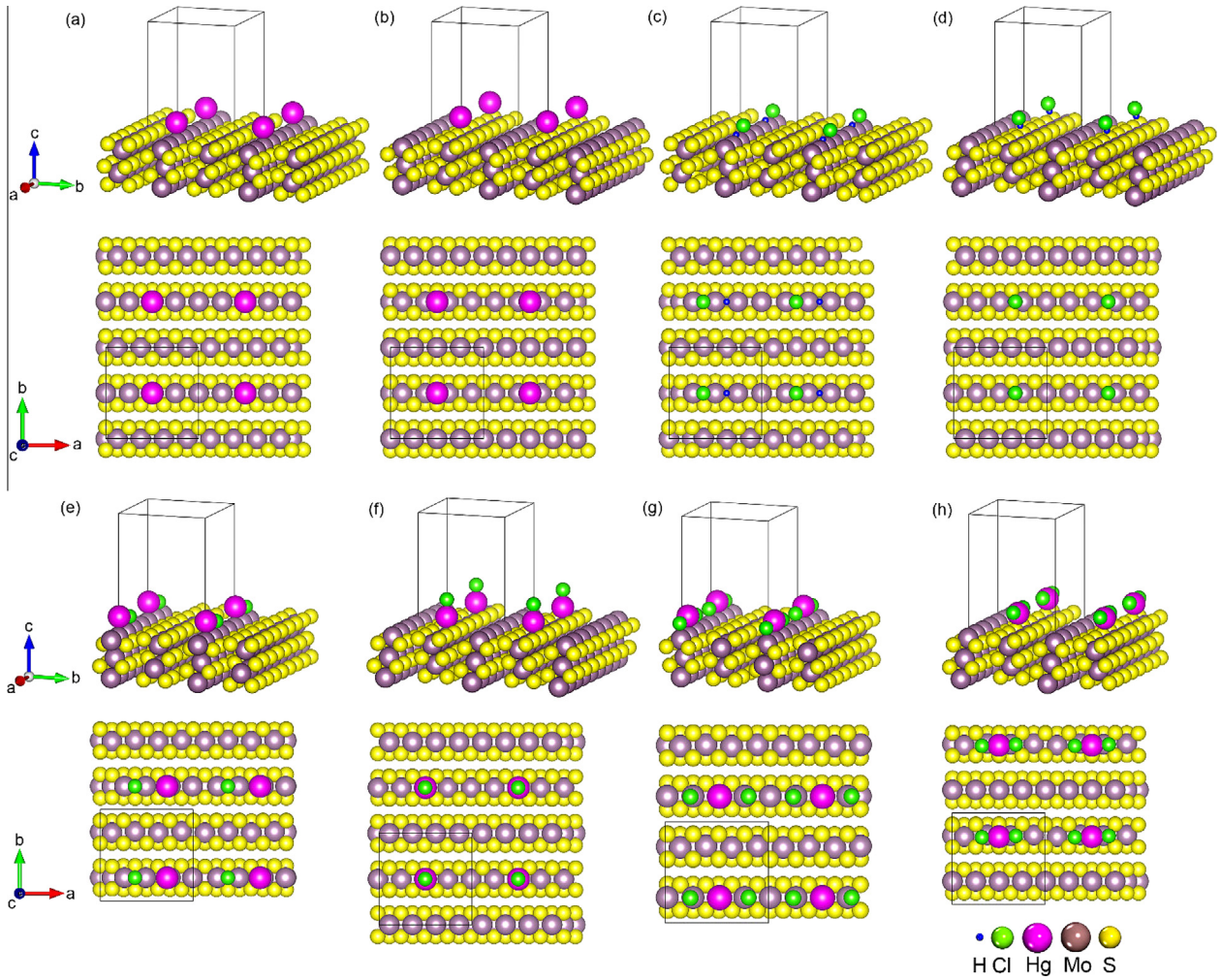

Fig. 1. Side and 3D view of the optimized stable configurations of Hg, HCl, HgCl and $HgCl_2$ adsorptions on (a) (c) (e) and (g) Mo top site, (b) (d) (f) and (h) S top site of MoS_2 (1 0 0) surface $p(4 \times 1)$ MoS_2 (1 0 0) surface (black line area).

Table 1
Adsorption energies E_{ads} (in eV/atom (Hg)), bond lengths d (in Å), Mulliken charges Q (in *e*), and bond population B of Hg adsorption on the MoS_2 (1 0 0) surface.

Adsorption site	E_{ads}	$d_{Mo(S)-Hg}$	Q_{Hg}	$B_{Mo(S)-Hg}$
Mo	−1.66	2.76	0.16	0.49
S	−0.92	3.46	0.03	0

charges transfer (0.03–0.16 *e*) from Hg to the MoS_2 surface. Moreover, the bond population (0.49) of Hg–Mo formed by Hg adsorption on the Mo top site of MoS_2 (1 0 0) surface is larger and positive, demonstrating that Hg atom is chemically adsorbed on the Mo top site. While for case of Hg adsorption on the S top site of MoS_2 (1 0 0) surface, the bond population of Hg–S is zero, which is consistent with the small Mulliken charge (0.03 *e*) of Hg atom. It also means that Hg adsorption on the S top site of MoS_2 (1 0 0) surface is a weak chemisorption process with an adsorption energy of −0.92 eV (−88.72 kJ/mol). Generally, the heat of chemisorption is in the range of 40–400 kJ/mol [58,59].

To gain deeper insights into the mechanism of mercury adsorption on the MoS_2 surface, the density of states (DOS) of the surface-adatom complex was calculated. The calculated partial density of states (PDOS) of MoS_2 bulk, clean MoS_2 (1 0 0) surface, MoS_2 (1 0 0) surface adsorbed with Hg atom are presented in Fig.2. Viewed from Fig. 2a, the isolated mercury atom before adsorption is distinguished by the distinct peak of *d* and *s* state about −3.2 and 0 eV, respectively, and an empty *p* state about 6.0 eV. Seen from Fig. 2b, after Hg adsorption on the Mo top site of MoS_2 (1 0 0) surface, all the electron states of Hg atom shift to red with the *s* state markedly broaden and the *s* and *p* state lower in energy, demonstrating the strong interactions between the Hg adatom and MoS_2 (1 0 0) substrate. As shown in Fig. 2d and e, after Hg adsorption all the *s*, *p* and *d* state of those Mo atoms adsorbed with Hg atom shift downward from 3 to 1.2 eV. The *s* and *p* state of Mo atoms shift to the lower energy level and are in hybridization with the *s*, *p*, and *d* state of Hg atom. The most prominent feature of the Hg *s* and *d* states is the peak located at −4 and −7 eV, respectively, corresponding to the local major peak of the Mo *s* and *d* states, respectively. The tremendous overlaps between the *s* and *p* states of Hg and the *s* and *p* states of Mo illustrate a strong reactivity of Hg adsorption on the top Mo atom site of MoS_2 (1 0 0) surface.

For cases of Hg adsorption on the top S site of MoS_2 (1 0 0) surface, PDOS in Fig. 2a and c indicate that all the electron states of Hg atom slightly change except for the attenuation of its unfilled *s* and *p* states, and the *s* and *p* states of the sulfur atom absorbed with a Hg atom in the energy level from −6 to 0 eV also have no marked change (Fig. 2f and g). All these evidences indicate that the interactions between Hg adatoms and those S atoms of MoS_2 (1 0 0) surface are relatively weak, which is consistent with the analysis of the corresponding adsorption energy, Mulliken charges and bond population.

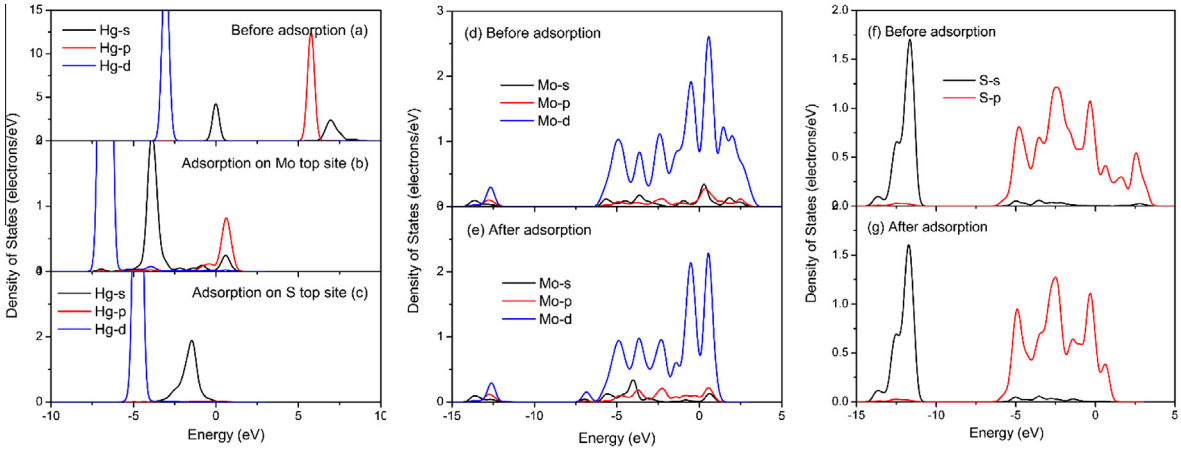

Fig. 2. PDOS of *s*, *p* and *d* states for Hg atom in (a) isolated Hg before adsorption. Hg adsorption on (b) the Mo top site; (c) the S top site of MoS_2 (1 0 0). PDOS of *s*, *p* and *d* states for Mo atom in (d) clean MoS_2 (1 0 0) surface and (e) top Mo adsorbed with Hg in MoS_2 (1 0 0). PDOS of *s* and *p* states for S atom in (f) clean MoS_2 (1 0 0) surface and (g) top S adsorbed with Hg in MoS_2 (1 0 0). Fermi energy level is set to zero.

3.2. HCl dissociated adsorption on MoS_2 (1 0 0) surface

Under the coal-fired flue gas environment, HCl plays the most significant oxidizing role in Hg^0 oxidation reaction due to its larger concentration than Cl_2 (the equilibrium concentration of Cl_2 is only ~1% of the HCl concentration) [24,26,60,61]. Thus, investigating the interaction between HCl molecule and MoS_2 (1 0 0) surface is indeed necessary for deep understanding the influence of HCl in the Hg catalytic oxidation reaction. The total catalytic oxidation reaction of Hg^0 with HCl is shown in the following equation:

$$Hg^0 + 2HCl + 1/2O_2 \rightarrow HgCl_2 + H_2O \quad (2)$$

The adsorption of HCl on the MoS_2 (1 0 0) surface was investigated by initially placing a single HCl molecule above those possible sites with its bond axis parallel or vertical to the surface. Then full optimizations of the fractional coordinates for these HCl absorption periodic models were performed. The optimized configurations of HCl adsorption on the MoS_2 (1 0 0) surface are depicted in Fig. 1c and d. Table 2 lists the calculated adsorption energy, bond length, Mulliken charge, and bond population of the MoS_2 (1 0 0) surface system adsorbed with an HCl molecule.

The stability of these HCl adsorption complexes follows this order: Mo top site > S edge site, which is in accordance with the order of Hg adsorption. The adsorption energy of HCl adsorption on the Mo top site of MoS_2 (1 0 0) surface is −3.95 eV/molecule (HCl), corresponding to a chemisorption process. The H–Cl bond is dramatically stretched from 1.28 Å (of gaseous HCl) to 3.26 Å, and the bond population of H–Cl is none, indicating the H–Cl covalent bond is fully destroyed after HCl adsorption on MoS_2 (1 0 0) surface. The bond length of Cl–Mo is 2.60 Å, and the corresponding bond population is 0.35, suggesting that Cl atom in HCl molecule is bonded to the Mo atom of MoS_2 (1 0 0) surface. The adsorption energy of HCl adsorption on the S top site is −0.94 eV, much higher than that case of HCl adsorption on the Mo top site. Here, H atom of the HCl molecule is bonded to the S atom with a negligible bond population (H–S) of 0.01, while the bond population of H–Cl is 0.67. Additionally, the H–Cl bond length is slightly elongated from 1.28 Å (in gaseous HCl) to 1.30 Å. All these evidences mean that after adsorption the H–Cl bond is completely destroyed and HCl adsorption on the Mo top site is a strong chemisorption process, while HCl adsorption on the S edge sites is a weak chemisorption process with few charge transfer and the intact H–Cl bond.

3.3. HgCl and $HgCl_2$ adsorption on MoS_2 (1 0 0) surface

Similarly, the adsorptions of HgCl and $HgCl_2$ on the MoS_2 (1 0 0) surface were examined by placing a single HgCl ($HgCl_2$) molecule on the different sites with its bond axis parallel and vertical to the MoS_2 (1 0 0) surface. Then full optimizations of the fractional coordinates for these HgCl ($HgCl_2$) absorption periodic models were performed. The optimized configurations of HgCl and $HgCl_2$ adsorption on MoS_2 (1 0 0) surface are depicted in Fig. 1e–h. Table 3 lists the calculated adsorption energy, bond length, Mulliken charge, and bond population of HgCl and $HgCl_2$ adsorption on the MoS_2 (1 0 0) surface, respectively.

By calculations, it is found that the Mo top site of the MoS_2 (1 0 0) surface is the preferred site for HgCl and $HgCl_2$ adsorption (Fig. 1e and g). For case of HgCl adsorption, the adsorption energy is −5.60 eV for the Mo top site and −2.87 eV for the S edge site, indicating that HgCl is strongly bonded to the Mo top site with an adsorption bond length of 2.77 Å (Mo–Hg) and 2.50 Å (Mo–Cl). However, the Hg–Cl bond is significantly elongated from 2.52 Å (of gaseous HgCl) to 4.41 Å, which shows that the Hg–Cl bond is fully destroyed after HgCl adsorption. Thus, the HgCl adsorption above the Mo site of MoS_2 (1 0 0) surface is a dissociative chemisorption. This most favorable adsorption is due to Hg and Cl atom are chemically bonded to the Mo atoms on the MoS_2 (1 0 0) surface with larger bond populations (see Table 3). When $HgCl_2$ adsorption on the Mo top site, Hg–Cl bond is significantly elongated from 2.42 Å (of gaseous HgCl) to 3.58 Å, corresponding to a dissociative chemisorption with a large adsorption energy of −5.97 eV/Hg atom.

While the adsorption energy of HgCl adsorption on the S edge site is −2.87 eV with an adsorption bond length (Hg–S) of 2.88 Å,

Table 2
Adsorption energies E_{ads} (in eV/molecule (HCl)), bond lengths d (in Å), Mulliken charges Q (in *e*), and bond population B of HCl adsorption on the MoS_2 (1 0 0) surface.

Adsorption site	E_{ads}	d	d_{H-Cl}	Q_H	Q_{Cl}	B_{H-Cl}	B
Mo	−3.95	2.60(Mo–Cl)	3.26	−0.26	−0.24	–	0.35 (Mo–Cl)
S	−0.94	2.65(H–S)	1.30	0.21	−0.28	0.67	0.01(H–S)

Table 3
Adsorption energies E_{ads} (in eV/molecule (HgCl or $HgCl_2$)), bond lengths (in Å), Mulliken charges Q (in *e*), and bond population of HgCl and $HgCl_2$ adsorption on the MoS_2 (1 0 0) surface.

	Adsorption site	E_{ads}	Bond length	Q_{Hg}	Q_{Cl}	Bond population		
HgCl	Mo	−5.60	2.77(Mo–Hg)	2.50(Mo–Cl)	0.18	−0.24	0.49(Mo–Hg)	0.29(Mo–Cl)
	S	−2.87	2.88(S–Hg)	2.36(Hg–Cl)	0.47	−0.40	0.07(S–Hg)	0.52(Hg–Cl)
$HgCl_2$	Mo	−5.97	2.79(Mo–Hg)	2.31(Mo–Cl)	0.21	−0.27	0.51(Mo–Hg)	0.60(Mo–Cl)
	S	−1.08	2.33(Hg–Cl1 or Cl2)	3.27(Hg–S)	0.63	−0.39	0.47(Hg–Cl1 or Cl2)	0(Hg–S)

and the bond length of Hg–Cl is 2.36 Å, slightly less than 2.52 Å of gaseous HgCl. Therefore, it is found that HgCl adsorption on the S edge site of MoS_2 (1 0 0) surface still keep the molecular configuration of gaseous HgCl. For case of $HgCl_2$ adsorption on the S edge site, the optimized configuration of $HgCl_2$ almost remains parallel to the MoS_2 (1 0 0) surface (Fig. 1h), and the angle of Cl–Hg–Cl reduces from 180° (of gaseous $HgCl_2$) to 158.9°. The $HgCl_2$ adsorption energy is −1.08 eV (−104.16 kJ/mol) with an Hg–Cl bond population of 0.47 and a bond length of 2.33 Å, slightly less than 2.42 Å of gaseous $HgCl_2$, indicating that the moderate chemisorption process of $HgCl_2$ mainly occurs on the S edge site of MoS_2 (1 0 0) surface [58,59].

3.4. Reaction mechanism of Hg catalytic oxidation on MoS_2 (1 0 0) surface

Based on above analysis of HgCl and $HgCl_2$ adsorption, it can be suggested that the HgCl and $HgCl_2$ molecules are easy to form on the S edge site of MoS_2 (1 0 0) surface with the moderate adsorption intensity, while HgCl and $HgCl_2$ would completely dissociated adsorb on the Mo top site of MoS_2 (1 0 0) surface with the broken Hg–Cl bonds and larger adsorption energies. Usually, a simple gas–solid catalytic process is composed of adsorption, charge transfer and dissociative adsorption, where too large and small adsorption energies are not benefit to the adsorption and dissociative adsorption of the gas molecule [62]. Thus, in this section we mainly focused on the S edge site of the $p(5 \times 1)$ MoS_2 (1 0 0) surface with the moderate adsorption intensity for the reaction pathway of Hg catalytic oxidation. For Hg oxidation pathway analysis, the configuration of one atomic Hg and two HCl molecules far from the clean MoS_2 (1 0 0) surface and the configuration of two atomic H bonded to S atoms in MoS_2 (1 0 0) surface and one $HgCl_2$ molecule far from the MoS_2 (1 0 0) surface were treated as the initial and final configurations (IM0 and FS) of Hg oxidation species on the MoS_2 (1 0 0) surface, respectively. Two main paths for Hg oxidation on the MoS_2 (1 0 0) surface were investigated and depicted in Fig. 3. The Hg oxidation pathway-I goes via two steps: Hg (ads) + Cl (ads) → HgCl (ads) → $HgCl_2$ (ads). The pathway-II directly goes via one step: Hg (ads) + 2Cl (ads) → $HgCl_2$ (ads). Here, all calculated energies of the Hg oxidation species, including the optimized intermediate (IM), transition state (TS) and final state (FS), are relative to the initial configuration of IM0, whose energy is set to zero. The structures of IM, TS and FS in the Hg catalytic oxidation process on the MoS_2 (1 0 0) surface are depicted in Fig. 4. Evolutions of Mulliken charges for Hg atom during two Hg catalytic oxidation pathways are provided in Fig. S1 (in Supporting Information).

For case of Hg oxidation reaction, firstly, one Hg and two HCl molecules adsorption on the MoS_2 (1 0 0) surface via IM0 → IM1 is exothermic by 61.13 kJ/mol, losing 0.105*e* of Hg atom (Fig. S1). Then Hg oxidation reaction is divided into two pathways. The pathway-I of Hg oxidation is via the route of IM1 → TS1 → IM2 → TS2 → IM3 containing two steps: (i) Hg → HgCl and (ii) HgCl → $HgCl_2$. The first Hg oxidation step of Hg → HgCl is endothermic by 25.27 kJ/mol with an energy barrier of 50.99 kJ/mol. In IM1, Hg atom is adsorbed on S edge site and H atoms of HCl molecules are also on the S edge site. Then, one Cl atom dissociates from the HCl molecule and is close to the Hg atom, creating a transition state of TS1 with the distance decreases: 2.34/1.28 Å (between H and S) and increases slightly: 3.28/3.36 Å (between Hg and S). From IM1 to TS1, Hg atom further loses 0.08*e*. Over TS1, in the intermediate of IM2, the S–Hg–Cl complex is created on the MoS_2 (1 0 0) surface with a Hg–Cl bond length of 2.6 Å, much close to 2.52 Å in gaseous HgCl, suggesting the creation of HgCl. Correspondingly, the bond length of Hg–S decreases: 3.36 Å in TS1, and 2.77 Å in IM2. The Mulliken charge of Hg atom in IM2 is 0.39*e*, indicating an acceerative Hg oxidation in the presence of HCl.

The second Hg oxidation step of HgCl → $HgCl_2$ via the IM2 → TS2 → IM3 is endothermic by 7.06 kJ/mol. The corresponding energy barrier is 44.62 kJ/mol smaller than 50.99 kJ/mol of the first

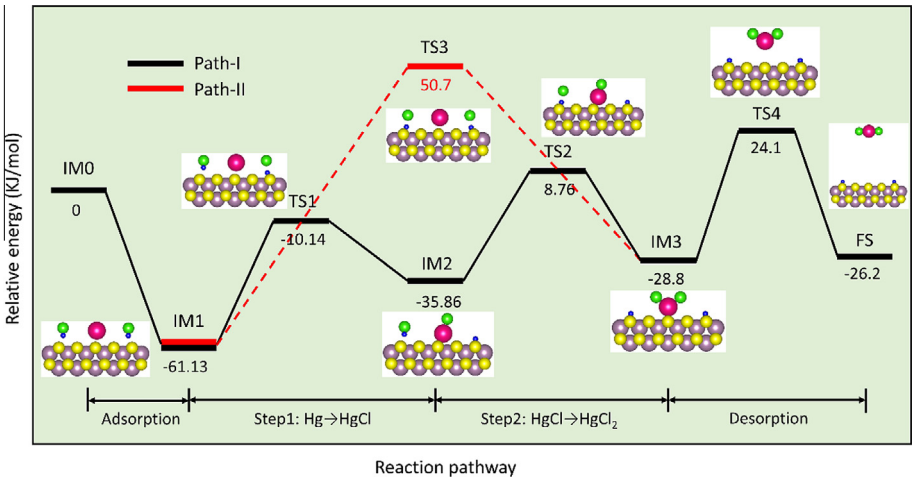

Fig. 3. Reaction pathways and energy profiles of Hg catalytic oxidation process on the MoS_2 (1 0 0) surface.

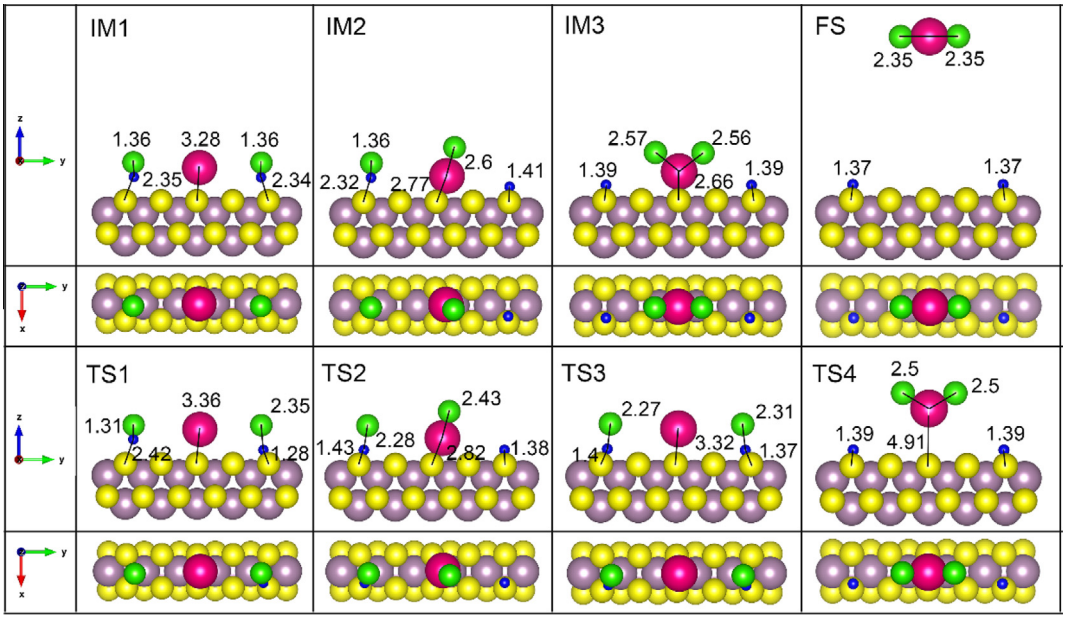

Fig. 4. Side and top views of the structures of intermediates, transition states, and final states in Hg catalytic oxidation pathways on MoS_2 (1 0 0) surface. (Mo, dark grey; S, yellow; Hg, red; H, blue; and Cl, green).

step, indicating the first oxidation step of Hg → HgCl is the rate-limiting step for the Hg catalytic oxidation. In the following step of IM2 → TS2, another Cl atom dissociates from the HCl molecule and approaches the formed HgCl molecule, forming a transition state of TS2 with the distance decreases: 2.6/2.43 Å (between Hg and Cl), 2.32/1.43 Å (between H and S) and increases slightly: 2.77/2.82 Å (between Hg and S). Over TS2, the intermediate IM3, the S–Hg–2Cl complex created on the MoS_2 (1 0 0) surface with two Hg–Cl bond lengths of 2.56 and 2.57 Å, much close to 2.52 Å in gaseous HgCl, indicating the formation of $HgCl_2$. During this step, the bond length of Hg–S decreases: 2.82 Å in TS2, and 2.66 Å in IM3. From IM2 to IM3, Hg atom further loses extra 0.047*e* with the presence of another HCl. Finally, an $HgCl_2$ molecule dissociates from the MoS_2 (1 0 0) surface via TS4 needing an energy of 2.6 kJ/mol with an energy barrier of 52.9 kJ/mol.

Moreover, the Pathway-II (Hg → $HgCl_2$) via the route of IM1 → TS3 → IM3 is an unfavorable oxidation pathway with an abrupt charge transfer of 0.237*e* for Hg atom, whose energy barrier is more than 111.83 kJ/mol. The whole catalytic oxidation reaction of IM0 →IM1 → TS1 → IM2 → TS2 → IM3 → TS4 → FS is exothermic by 26.2 kJ/mol. Comparing to these two oxidation pathways, the distributed pathway of Hg → HgCl → $HgCl_2$ is the most favorable pathway for Hg catalytic oxidation, rather than the directly oxidizing pathway of Hg → $HgCl_2$. Moreover, the rate-limiting steps are the first oxidation step of Hg → HgCl and the last step of $HgCl_2$ molecule desorbing from the MoS_2 (1 0 0) surface, i.e., the formation of HgCl and the dissociation of $HgCl_2$. For those adsorbed H atoms on the MoS_2 (1 0 0) surface, they would combine with O_2 to form H_2O molecules, subsequently escape from the MoS_2 surface [63].

Furthermore, it's necessary and meaningful to compare this case of Hg catalytic oxidation on the MoS_2 (1 0 0) surface to that on other catalyst surfaces such as Au (1 1 1) [19,20], Pd (1 0 0) [5], MnO_2 (1 1 0) [26,64], CeO_2 (1 1 1) [24] and V_2O_5/TiO_2 (0 0 1) [25,60]. Furthermore, many experimental researches have verified the high efficiency of Au, Pd and V_2O_5/TiO_2 catalysts for the oxidation of Hg^0 to Hg^{2+} [4,7]. Hg oxidation on Au (1 1 1) surface undergoes by the Langmuir–Hinshelwood (L–H) and prefers the pathway of Hg → HgCl → $HgCl_2$, which is consistent with the case of Hg oxidation on MoS_2 (1 0 0) surface. Hg oxidation on the Pd (1 0 0) surface also obeys the L–H mechanism, in which Hg adsorbs and then reacts with two HCl molecules that have previously been adsorbed and dissociated on the Pd(1 0 0) surface. More interestingly, the formation of $HgCl_2$ prefers the direct pathway of Hg (ads) + 2HCl (ads) → $HgCl_2$ (ads) for Hg oxidation on the Pd (1 0 0) surface [5]. However, comparing to V_2O_5/TiO_2, it is found that Hg can be oxidized on the V_2O_5/TiO_2 surface via the E–R mechanism due to Hg physical adsorption on the V_2O_5/TiO_2 surface. For all above cases, the formation reaction of $HgCl_2$ with a higher barrier is the rate-determining step. For example, barrier of $HgCl_2$ formation on the Au (1 1 1) surface is from 33 to 55 kJ/mol [19,20], Pd (1 0 0) surface is 67.53 kJ/mol [5], MnO_2 (1 1 0) surface is 66.27 kJ/mol [26,64], CeO_2 (1 1 1) surface is 59.39 kJ/mol [24] and V_2O_5/TiO_2 (0 0 1) surface is 91.53 kJ/mol [25,60].

From above analysis, for Hg catalytic oxidation reaction on MoS_2 (1 0 0) surface, the rate-limiting steps are the first oxidation step of Hg → HgCl with barrier of 50.99 kJ/mol and the last step of $HgCl_2$ molecule dissociating from the MoS_2 (1 0 0) surface with barrier of 52.9 kJ/mol. Although, the rate-limiting step of Hg oxidation on MoS_2 (1 0 0) surface is different from above cases of second oxidation step of HgCl → $HgCl_2$, our calculated barrier of the rate-determining step on the MoS_2 (1 0 0) surface is slightly higher than that on Au (1 1 1), but lower than that on Pd (1 0 0), MnO_2 (1 1 0), CeO_2 (1 1 1) and V_2O_5/TiO_2 (0 0 1). The low energy barrier for mercury oxidation over the MoS_2 (1 0 0) surface make it an attractive catalysts for Hg catalytic oxidation.

4. Conclusions

To gain a fundamental understanding of the mercury oxidation mechanism on MoS_2 (1 0 0) surface, first-principles calculations based on the density functional theory (DFT) and the periodic slab models were carried out. The adsorptions of Hg^0, HCl, HgCl, and $HgCl_2$ on the MoS_2 (1 0 0) surface were all investigated. The electronic structures of surface system before and after adsorption were studied for the better understanding of the surface reactivity. The overlap between the *s*, *p* state of Hg and the *s*, *p* state of Mo

atom makes Hg^0 strongly adsorb on Mo top site of the MoS_2 (1 0 0) surface. HCl adsorption on MoS_2 (1 0 0) surface is a chemical dissociated process with the broken H–Cl bonds, which is essential for the Hg^0 oxidation reaction on the MoS_2 (1 0 0) surface. HgCl and $HgCl_2$ is adsorbed dissociatively on the Mo top site, while adsorbed non-dissociatively on the S edge site of MoS_2 (1 0 0) surface. Energy pathway reveals that Hg oxidation on the MoS_2 (1 0 0) surface follows the Langmuir–Hinshelwood mechanism, in which the oxidation of adsorbed Hg^0 undergoes via the pathway of Hg → HgCl → $HgCl_2$. In the whole Hg oxidation reaction, the formation of HgCl and the dissociation of $HgCl_2$ are the rate-determining steps due to their higher energy barriers. The lower energy barrier for mercury oxidation reaction on MoS_2 (1 0 0) than Pd (1 0 0), MnO_2 (1 1 0), CeO_2 (1 1 1) and V_2O_5/TiO_2 (0 0 1) make it an attractive alternative catalyst for Hg catalytic oxidation.

Acknowledgments

We sincerely acknowledge the High Performance Computing Center of CSU, China. This work was financially supported by the National Science and Technology Support Project of China (No. 2012BAE08B02).

Appendix A. Supplementary data

Supplementary data associated with this article can be found, in the online version, at http://dx.doi.org/10.1016/j.cej.2016.10.059.

References

[1] E.G. Pacyna, J.M. Pacyna, F. Steenhuisen, S. Wilson, Global anthropogenic mercury emission inventory for 2000, Atmos. Environ 40 (2006) 4048–4063.
[2] E.G. Pacyna, J.M. Pacyna, K. Sundseth, J. Munthe, K. Kindbom, S. Wilson, F. Steenhuisen, P. Maxson, Global emission of mercury to the atmosphere from anthropogenic sources in 2005 and projections to 2020, Atmos. Environ. 44 (2010) 2487–2499.
[3] S.J. Wilson, F. Steenhuisen, J.M. Pacyna, E.G. Pacyna, Mapping the spatial distribution of global anthropogenic mercury atmospheric emission inventories, Atmos. Environ. 40 (2006) 4621–4632.
[4] S. Wang, L. Zhang, B. Zhao, Y. Meng, J. Hao, Mitigation Potential of Mercury Emissions from Coal-Fired Power Plants in China, Energy Fuels 26 (2012) 4635–4642.
[5] B. Zhang, J. Liu, J. Zhang, C. Zheng, M. Chang, Mercury oxidation mechanism on Pd(1 0 0) surface from first-principles calculations, Chem. Eng. J. 237 (2014) 344–351.
[6] J. Liu, W. Qu, C. Zheng, Theoretical studies of mercury–bromine species adsorption mechanism on carbonaceous surface, Proc. Combust. Inst. 34 (2013) 2811–2819.
[7] J. Wilcox, E. Rupp, S.C. Ying, D.-H. Lim, A.S. Negreira, A. Kirchofer, F. Feng, K. Lee, Mercury adsorption and oxidation in coal combustion and gasification processes, Int. J. Coal Geol. 90–91 (2012) 4–20.
[8] W. Lee, G.N. Bae, Removal of elemental mercury (hg(0)) by nanosized V_2O_5/TiO_2 catalysts, Environ. Sci. Technol. 43 (2009) 1522–1527.
[9] Y. Zhao, J. Zhang, J. Liu, M. Díaz-Somoano, P. Abad-Valle, M.R. Martínez-Tarazona, C. Zheng, Experimental study on fly ash capture mercury in flue gas, Sci. China Technol. Sci. 53 (2010) 976–983.
[10] A.D. Jew, E.C. Rupp, D.L. Geatches, J.-E. Jung, G. Farfan, L. Bahet, J.C. Hower, G.E. Brown Jr., J. Wilcox, Mercury interaction with the fine fraction of coal-combustion fly ash in a simulated coal power plant flue gas stream, Energy Fuels 29 (2015) 6025–6038.
[11] E.S.A.J. Wilcox, Mercury species and SO2 adsorption on CaO(100), J. Phys. Chem. C 112 (2008) 16484–16490.
[12] C.C. Gilmour, G.S. Riedel, G. Riedel, S. Kwon, R. Landis, S.S. Brown, C.A. Menzie, U. Ghosh, Activated carbon mitigates mercury and methylmercury bioavailability in contaminated sediments, Environ. Sci. Technol. 47 (2013) 13001–13010.
[13] E.A. Morris, D.W. Kirk, C.Q. Jia, K. Morita, Roles of sulfuric acid in elemental mercury removal by activated carbon and sulfur-impregnated activated carbon, Environ. Sci. Technol. 46 (2012) 7905–7912.
[14] K.S. Kumar Reddy, A. Al Shoaibi, C. Srinivasakannan, Sulfur-leaching facts from sulfur-impregnated porous carbons in the mercury removal process, Energy Fuels 29 (2015) 4488–4491.
[15] X. Li, Z. Liu, J.Y. Lee, Adsorption kinetic and equilibrium study for removal of mercuric chloride by $CuCl_2$-impregnated activated carbon sorbent, J. Hazard. Mater. 252–253 (2013) 419–427.
[16] P. Hadi, M.H. To, C.W. Hui, C.S. Lin, G. McKay, Aqueous mercury adsorption by activated carbons, Water Res. 73 (2015) 37–55.
[17] D. Karatza, A. Lancia, M. Prisciandaro, D. Musmarra, G. Mazziotti di Celso, Influence of oxygen on adsorption of elemental mercury vapors onto activated carbon, Fuel 111 (2013) 485–491.
[18] J.-E. Jung, D. Geatches, K. Lee, S. Aboud, G.E. Brown, J. Wilcox, First-Principles Investigation of Mercury Adsorption on the α-$Fe_2O_3(1\bar{1}\ 0\ 2)$ Surface, J. Phys. Chem. C 119 (2015) 26512–26518.
[19] D.H. Lim, J. Wilcox, Heterogeneous mercury oxidation on Au(1 1 1) from first principles, Environ. Sci. Technol. 47 (2013) 8515–8522.
[20] D.H. Lim, S. Aboud, J. Wilcox, Investigation of adsorption behavior of mercury on Au(1 1 1) from first principles, Environ. Sci. Technol. 46 (2012) 7260–7266.
[21] L. Geng, L. Han, W. Cen, J. Wang, L. Chang, D. Kong, G. Feng, A first-principles study of Hg adsorption on Pd(1 1 1) and Pd/γ-Al_2O_3(1 1 0) surfaces, Appl. Surf. Sci. 321 (2014) 30–37.
[22] Shela Aboud, Erdem Sasmaz, J. Wilcox, Mercury adsorption on PdAu, PdAg and PdCu alloys, Main Group Chem. 7 (2008) 205–215.
[23] E.S. Olson, S.J. Miller, R.K. Sharma, G.E. Dunham, S.A. Benson, Catalytic effects of carbon sorbents for mercury capture, J. Hazard. Mater. 74 (2000) 61–79.
[24] B. Zhang, J. Liu, F. Shen, Heterogeneous mercury oxidation by HCl over CeO_2 catalyst: density functional theory study, J. Phys. Chem. C 119 (2015) 15047–15055.
[25] J. Liu, M. He, C. Zheng, M. Chang, Density functional theory study of mercury adsorption on V_2O_5 (0 0 1) surface with implications for oxidation, Proc. Combust. Inst. 33 (2011) 2771–2777.
[26] B. Zhang, J. Liu, Y. Yang, M. Chang, Oxidation mechanism of elemental mercury by HCl over MnO_2 catalyst: insights from first principles, Chem. Eng. J. 280 (2015) 354–362.
[27] L. Tao, X. Guo, C. Zheng, Density functional study of Hg adsorption mechanisms on α-Fe_2O_3 with H2S, Proc. Combust. Inst. 34 (2013) 2803–2810.
[28] S. Sun, D. Zhang, C. Li, Y. Wang, Q. Yang, Density functional theory study of mercury adsorption and oxidation on CuO(1 1 1) surface, Chem. Eng. J. 258 (2014) 128–135.
[29] W. Xiang, J. Liu, M. Chang, C. Zheng, The adsorption mechanism of elemental mercury on CuO (1 1 0) surface, Chem. Eng. J. 200–202 (2012) 91–96.
[30] T. Liu, L. Xue, X. Guo, C.-G. Zheng, DFT study of mercury adsorption on α-Fe_2O_3 surface: role of oxygen, Fuel 115 (2014) 179–185.
[31] A. Suarez Negreira, J. Wilcox, DFT study of Hg oxidation across Vanadia-Titania SCR catalyst under flue gas conditions, J. Phys. Chem. C 117 (2013) 1761–1772.
[32] A. Suarez Negreira, J. Wilcox, Role of WO_3 in the Hg oxidation across the V_2O_5–WO_3–TiO_2 SCR catalyst: a DFT study, J. Phys. Chem.. C 117 (2013) 24397–24406.
[33] Y.H. Lee, X.Q. Zhang, W. Zhang, M.T. Chang, C.T. Lin, K.D. Chang, Y.C. Yu, J.T. Wang, C.S. Chang, L.J. Li, T.W. Lin, Synthesis of large-area MoS_2 atomic layers with chemical vapor deposition, Adv. Mater. 24 (2012) 2320–2325.
[34] K.K. Liu, W. Zhang, Y.H. Lee, Y.C. Lin, M.T. Chang, C.Y. Su, C.S. Chang, H. Li, Y. Shi, H. Zhang, C.S. Lai, L.J. Li, Growth of large-area and highly crystalline MoS_2 thin layers on insulating substrates, Nano Lett. 12 (2012) 1538–1544.
[35] D. Kong, H. Wang, J.J. Cha, M. Pasta, K.J. Koski, J. Yao, Y. Cui, Synthesis of MoS_2 and $MoSe_2$ films with vertically aligned layers, Nano Lett. 13 (2013) 1341–1347.
[36] A.J.Z.O. Kourosh Kalantar-Zadeh, Biosensors based on two-dimensional MoS2, ACS Sensors 1 (2016) 5–16.
[37] Min-Rui Gao, Jin-Xia Liang, Ya-Rong Zheng, Yun-Fei Xu, Jun Jiang, Qiang Gao, Jun Li, Shu-Hong Yu, An efficient molybdenum disulfide/cobalt diselenide hybrid catalyst for electrochemical hydrogen generation, Nat. Commun. 6 (2015) 5982, http://dx.doi.org/10.1038/ncomms6982.
[38] Y. Li, D. Wu, Z. Zhou, C.R. Cabrera, Z. Chen, Enhanced Li Adsorption and Diffusion on MoS2 Zigzag Nanoribbons by Edge Effects: A Computational Study, J. Phys. Chem. Lett. 3 (2012) 2221–2227.
[39] M. Mortazavi, C. Wang, J. Deng, V.B. Shenoy, N.V. Medhekar, Ab initio characterization of layered MoS_2 as anode for sodium-ion batteries, J. Power Sources 268 (2014) 279–286.
[40] W.H. Ryu, J.W. Jung, K. Park, S.J. Kim, I.D. Kim, Vine-like MoS_2 anode materials self-assembled from 1-D nanofibers for high capacity sodium rechargeable batteries, Nanoscale 6 (2014) 10975–10981.
[41] V.P. Santos, B. van der Linden, A. Chojecki, G. Budroni, S. Corthals, H. Shibata, G. R. Meima, F. Kapteijn, M. Makkee, J. Gascon, Mechanistic insight into the synthesis of higher alcohols from Syngas: the role of K promotion on MoS_2 catalysts, ACS Catal. 3 (2013) 1634–1637.
[42] A. Andersen, S.M. Kathmann, M.A. Lilga, K.O. Albrecht, R.T. Hallen, D. Mei, Adsorption of potassium on MoS_2(1 0 0) surface: a first-principles investigation, J. Phys. Chem. C 115 (2011) 9025–9040.
[43] A.S.M. Komarneni, U. Burghaus, Adsorption of thiophene on inorganic MoS_2 fullerene-like nanoparticles, Catal. Lett. 129 (2009) 66–70.
[44] Xiangyang Yanhong-Chao, W.Z. Wu, Fangfang Hou, Suhang Xun, Peiwen Wu, Haiyan Ji, Hui Xu, Huaming Li, Application of graphene-like layered molybdenum disulfide and its excellent adsorption behavior for doxycycline antibiotic, Chem. Eng. J. 243 (2014) 60–67.
[45] X.-R. Shi, S.-G. Wang, J. Hu, H. Wang, Y.-Y. Chen, Z. Qin, J. Wang, Density functional theory study on water–gas-shift reaction over molybdenum disulfide, Appl. Catal. A General 365 (2009) 62–70.
[46] H. Zhao, G. Yang, X. Gao, C.H. Pang, S.W. Kingman, T. Wu, Hg(0) capture over CoMoS/gamma-Al_2O_3 with MoS_2 nanosheets at low temperatures, Environ. Sci. Technol. 50 (2016) 1056–1064.
[47] P. Raybaud, J. Hafner, G. Kresse, S. Kasztelan, H. Toulhoat, Structure, energetics, and electronic properties of the surface of a promoted MoS_2 catalyst: an ab initio local density functional study, J. Catal. 190 (2000) 128–143.

[48] J.K.N. Line, S. Byskov, Bjerne S. Clausen, Henrik Topsøe, Henrik Topsøe, DFT calculations of unpromoted and promoted MoS2-based hydrodesulfurization catalysts, J. Catal. 187 (1999) 109–122.
[49] P. Raybaud, J. Hafner, G. Kresse, S. Kasztelan, H. Toulhoat, Ab initio study of the H2–H2S/MoS2 gas-solid interface: the nature of the catalytically active sites, J. Catal. 189 (2000) 129–146.
[50] H. Schweiger, P. Raybaud, G. Kresse, H. Toulhoat, Shape and edge sites modifications of MoS_2 catalytic nanoparticles induced by working conditions: a theoretical study, J. Catal. 207 (2002) 76–87.
[51] J.P. Perdew, K. Kieron, Matthias Ernzerhof, Generalized gradient approximation made simple, Phys. Rev. Lett. 77 (1996) 3865–3868.
[52] G. Kresse, Efficient iterative schemes for ab initio total-energy calculations using a plane-wave basis set, Phys. Rev. B 54 (1996) 169–186.
[53] Kari Laasonen, Roberto Car, Changyol Lee, David Vanderbilt, Implementation of ultrasoft pseudo potentials in ab initio molecular dynamics, Phys. Rev. B 43 (1991) 6796.
[54] H.J. Monkhorst, J.D. Pack, Special points for Brillouin-zone integrations, Phys. Rev. B 13 (1976) 5188.
[55] X. Lv, Z. Xu, J. Li, J. Chen, Q. Liu, Investigation of fluorine adsorption on nitrogen doped $MgAl_2O_4$ surface by first-principles, Appl. Surf. Sci. 376 (2016) 97–104.
[56] N. Govind, M. Petersen, G. Fitzgerald, D. King-Smith, J. Andzelm, A generalized synchronous transit method for transition state location, Comput. Mater. Sci. 28 (2003) 250–258.
[57] G. Henkelman, B.P. Uberuaga, H. Jónsson, A climbing image nudged elastic band method for finding saddle points and minimum energy paths, J. Chem. Phys. 113 (2000) 9901.
[58] W. Ji, Z. Shen, M. Fan, P. Su, Q. Tang, C. Zou, Adsorption mechanism of elemental mercury (Hg0) on the surface of $MnCl_2$ (1 1 0) studied by Density Functional Theory, Chem. Eng. J. 283 (2016) 58–64.
[59] J.D.P.P. Atkins, Physical Chemistry, Oxford University Press, CA, 2002, pp. 57–80.
[60] B. Zhang, J. Liu, G. Dai, M. Chang, C. Zheng, Insights into the mechanism of heterogeneous mercury oxidation by HCl over V_2O_5/TiO_2 catalyst: periodic density functional theory study, Proc. Combust. Inst. 35 (2015) 2855–2865.
[61] A.A. Presto, E.J. Granite, Noble metal catalysts for mercury oxidation in utility flue gas, Platinum Met. Rev. 52 (2008) 144–154.
[62] W.G. Ruibin, Jiang, Ming Li, Houyu Zhu, Jing Li, Lianming Zhao, Dianling Fu, and Honghong Shan, Density Functional Study of the Reaction of SO_2 on Ir(1 1 1), J. Phys. Chem. C 113 (2009) 18223–18232.
[63] R.R.M. Johnston, J.W. Moore, Water adsorption on molybdenum disulfide containing surface contaminants, J. Phys. Chem. 68 (1964) 3399–3406.
[64] B. Zhang, J. Liu, C. Zheng, M. Chang, Theoretical study of mercury species adsorption mechanism on MnO_2(1 1 0) surface, Chem. Eng. J. 256 (2014) 93–100.